Recording depth and signal competition in heterodyne interferometry

Ombeline de La Rochefoucauld,[a] Shyam M. Khanna,[b] and Elizabeth S. Olson[c]
Fowler Memorial Laboratory, Department of Otolaryngology, Head and Neck Surgery, College of Physicians and Surgeons of Columbia University, New York, New York 10032

(Received 14 June 2004; revised 11 November 2004; accepted 22 November 2004)

A common way to measure submicroscopic motion of the organ of Corti is heterodyne interferometry. The depth over which vibration can be accurately measured with heterodyne interferometry is determined by both the optics, which controls to what extent light from nonfocal planes reaches the photodetectors, and demodulation electronics, which determines to what extent signal generated by out-of-focal-plane light influences the measurements. The influence of a second reflecting surface is investigated theoretically and experimentally. By reviewing the theory of FM demodulation and showing tests with a Revox FM demodulator, it is demonstrated that the influence of a secondary signal on a measurement depends on the modulation index. Both high- and low-modulation index signals are encountered in heterodyne interferometry of the cochlea. Using a He–Ne-like diode laser ($\lambda = 638$ nm), the border between low- and high-modulation signals is at a displacement of about 25–100 nm. Confocal interferometry reduces the magnitude of out-of-focus signals, and therefore their effect on vibration measurement. The response of the confocal system to reflected signals from two surfaces separated by distances encountered within the cochlear partition is shown. The results underscore the benefit of steep optical sectioning for intracochlear measurements. © *2005 Acoustical Society of America.* [DOI: 10.1121/1.1848177]

PACS numbers: 43.64.Kc, 43.64.Yp Pages: 1267–1284

LIST OF SYMBOLS

f_o frequency of the object beam
f_r frequency of the reference beam
f_c carrier frequency
f_m modulation frequency
Δf frequency deviation
ω radial frequency $= 2\pi f$
λ wavelength of laser light
$V_A(t)$, $V_C(t)$ velocity of surface **A** or **C**
$x_A(t)$, $x_C(t)$ FM signal out of photodetector due to surface **A** or **C**
$\beta = 2\pi\Delta f/\omega_m$ modulation index,
V_o = velocity amplitude,
X_o = displacement amplitude
$\Delta f = 2V_o/\lambda = 2\omega_m X_o/\lambda$ frequency deviation in terms of object motion, due to Doppler shift
ψ_0 relative phase between FM signals $x_A(t)$, $x_C(t)$
a, c amplitudes of the FM signals $x_A(t)$, $x_C(t)$
ρ $= c/a$
$E(t)$ theoretical demodulator output signal
$E_o(t)$ experimental demodulator output signal from optical experiment
$E_g(t)$ experimental demodulator output signal from experiment with signal generators
R reflectivity
m relative interference amplitude (wavefront distortion)
k value the carrier power takes at a given distance from the plane of focus (from optical sectioning curve)
d distance between the two surfaces in the optical experiments
z distance from the focal plane

I. INTRODUCTION

Heterodyne interferometry has been the primary technique for measuring cochlear motion for some time (Willemin *et al.*, 1988, Nuttall *et al.*, 1991, Ruggero and Rich, 1991, Cooper, 1999a). The technique uses interference between two laser beams (object and reference) whose frequencies have been shifted from each other by an amount that can be resolved by standard electronics (455 kHz in our system). The velocity of the test object shifts the frequency of the object beam due to the Doppler effect and is encoded in the frequency modulation of the 455-kHz heterodyne ''carrier'' signal. The heterodyne signal is decoded using a frequency demodulator. (Equivalently, the displacement of the test object changes the distance through which the object beam travels, thus modulating the phase of the object beam. Displacement is decoded with a phase demodulator.) The cochlear tissues are of low reflectivity and, in order to in

[a]Author to whom correspondence should be addressed. Electronic mail: or2107@columbia.edu
[b]Electronic mail: smk3@columbia.edu
[c]Electronic mail: eao2004@columbia.edu

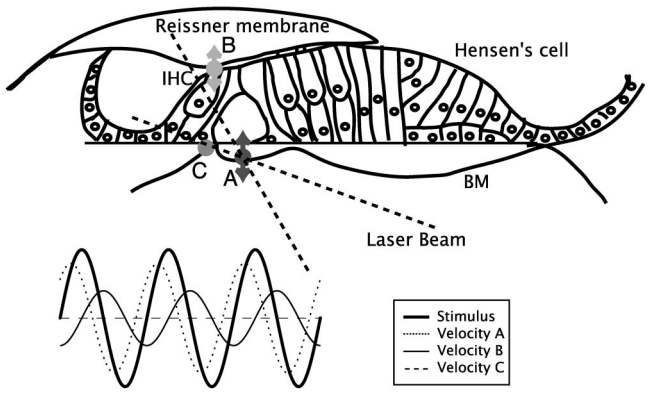

FIG. 1. The organ of Corti consists of several cellular and acellular layers. The measuring laser beam of the interferometer is therefore reflected from several surfaces. When sound is applied to the cochlea, these surfaces (for example, **A**: basilar membrane (BM); **B**: inner hair cell (IHC); **C**: lamina) vibrate with different amplitudes and phases. Individual reflections from these surfaces produce carrier signals of different amplitudes, phases, and Doppler shifts at the photodetector. The relative magnitude of the optical signals reaching the detector depends on the plane of focus of the interferometer, reflectivity and orientation of the surface, and on the optical sectioning characteristics of the interferometer. The frequency demodulator determines how much the out-of-plane reflections affect the vibration being measured.

crease the power in the object beam, reflecting beads are often placed on the sensory tissue and the motion of the beads measured. A bead is a retro-reflector and the light reflected from it comes from a well-defined depth. However, measurements with beads also have disadvantages: The position of measurement is restricted to that of the bead, and holes must be made in the overlying tissue in order to place the bead. The bead might or might not move with the underlying tissue (Khanna *et al.*, 1998, Cooper, 1999b). On the other hand, for measurements made without a bead, the laser beam goes through the tissue and means have to be provided in order to select the depth from which the reflection is accepted by the interferometer. For example, in Fig. 1 different parts of the sensory tissue are imagined to move with different amplitudes and phases. We would like to know under what conditions reflections from out-of-focus surfaces affect the measured velocity of the in-focus surface.

The accuracy with which vibration at a selected plane can be measured in the presence of reflections from secondary surfaces is determined by the optical sectioning characteristics of the interferometer and the signal processing of the FM demodulator. By reviewing the theory of FM demodulation and describing tests with our FM demodulator, we show that the influence of a secondary signal is qualitatively different depending on whether the modulation index is high (greater than 2) or low (less than 0.5). The modulation index, β, is the ratio of the frequency deviation to the modulation (stimulus) frequency ($\beta = \Delta f / f_m$). For perpendicular incidence, the frequency deviation is related to the magnitude of the velocity via a Doppler shift: $\Delta f = 2V_o/\lambda$, where $\lambda = 638$ nm for our laser. When the response to a pure-tone stimulus is linear, $V_o = \omega X_o$, where X_o = displacement and $\omega = 2\pi$ multiplied by the stimulus frequency, and thus $\beta = 4\pi X_o/\lambda$. Therefore, high modulation index corresponds to displacements greater than 100 nm, low modulation index corresponds to displacements less than 25 nm. Both high- and low-modulation-index signals occur in heterodyne interferometry of the cochlea. For high-modulation-index signals, the fundamental component of the output of the FM demodulator is not affected by a secondary signal unless the secondary signal's power is nearly as large as that of the primary signal. However, the output waveform can be distorted. For a low-modulation-index signal, a secondary competing signal can have a relatively large effect on the fundamental component of the output signal, but the output signal waveform is not distorted. Cells and structures in the cochlea have a wide range of reflectivities, and steep optical sectioning is necessary to reduce contamination by out-of-focus signals.

Detailed discussion on the spatial resolution of intracochlear velocity measurements appeared in two 2001 letters to the *Journal of the Acoustical Society*. These are Ren and Nuttall, 2001, ''Recording depth of the heterodyne laser interferometer for cochlear vibration measurement,'' and Dalhoff *et al.*, 2001, ''Remarks about the depth resolution of heterodyne interferometers in cochlear investigations.'' Our contribution concerns optical sectioning and FM demodulation, and continues the discussion of those letters.

In the article by Ren and Nuttall, a heterodyne interferometer was used to measure the velocity of a vibrating mirror. The optical sectioning curve shows the decrease of the power in the carrier signal as the distance between a reflective plane and the focal plane (the defocus distance) is increased. The FWHM is defined as the full width of the carrier power curve at half maximum. The recording depth can be defined as the defocus distance at which the reported velocity of the reflective plane decreases to 50%. Ren and Nuttall reported that the carrier power decreased to 50% of its maximum at a distance of $\sim \pm 9.5$ μm from the focal plane (FWHM $= 19.5$ μm), and to approximately 10% at a distance of ± 25 μm. At larger distances there was no further reduction of carrier power. In contrast, the measured velocity did not change with defocusing distances -40 to $+25$ μm. At distances of -60, $+35$ μm the velocity had dropped to 50% of its maximum. Because this total distance (95 μm) was much larger than the FWHM of 19.5 μm for the carrier, the authors noted that the FWHM for the carrier power could not be used to determine the FWHM for the velocity. Below, we further explore the relationship between depth resolution and optical sectioning.

The letter by Dalhoff *et al.* discussed the effect of a signal from a secondary reflector. As the letter states, the light waves from the primary and secondary reflectors will add at the input to the photodetector. In this contribution we extend the discussion of Dalhoff *et al.* by considering the subsequent processing of the summed signal. When reflections from two objects contribute to the light input to the photodetector, the output signal from the photodetector at the heterodyne frequency that feeds the FM demodulator is the sum of two signals, each with amplitude proportional to the square root of the light power from one of the reflectors. Each signal is frequency modulated by the Doppler shift that is proportional to the velocity of its reflector. The purpose of FM demodulation is to extract the instantaneous frequency of the frequency-modulated signal. Therefore, to analyze the

summed signal analytically, the instantaneous frequency of the summed signal is the quantity of interest. The analytic section of this paper shows the instantaneous frequency under various conditions and leads to the low-modulation-index, high-modulation-index classification of results. Tests with our FM demodulator with input signals produced with two signal generators are shown, and confirm the analytic results. Finally, we show the response of our integrated optical and demodulator system when the two competing signals are produced optically, by reflecting surfaces with realistic cochlea-like separations and motions. First we review the optical sectioning of the split-aperture system developed by Khanna *et al.* (1996), as the conclusions of the demodulation analysis and tests will point to the importance of steep optical sectioning for reducing the contamination from secondary reflectors.

II. MEASUREMENTS AND DISCUSSION

A. Optical sectioning

The optical sectioning capability of an optical system is its ability to select light from one plane in the illuminated sample and reject light from out-of-focus planes. The shape of the optical sectioning curve is governed by several factors: (I) The objective lens's numerical aperture (N.A.) determines the shape of the optical sectioning curve near the plane of focus. (II) Light returning from out-of-focus planes can be reduced by directly blocking it. This is how a slit confocal microscope works (Koester *et al.*, 1994). (III) A low coherence source (such as a low coherence diode laser or a superluminescent diode) can be used to reduce the contribution of light returning from out-of-focus planes. This strategy was described by Dalhoff *et al.* (2001).

The approximate analytic expression for the optical sectioning curve due to the objective lens's N. A. is

$$V(z)=\{\sin(Z)/Z\}^2, \quad Z=\pi(\text{N.A.})^2 z/n\lambda, \tag{1}$$

where $V(z)$ is proportional to the light power as a function of Z, n is the refractive index of the medium, N.A. is the numerical aperture of the lens, λ is the wavelength, and z is the distance from the focal plane. [Dalhoff *et al.* discuss the limitations of Eq. (1) and reference Wilson, 1990.] [As a clarifying note: When the object beam interferes with a reference beam in a heterodyne interferometer, the voltage out of the photodetector at the heterodyne frequency—the heterodyne signal—is proportional to the square root of Eq. (1), as only the object beam is passed through the objective lens. The power in the heterodyne signal, the ''carrier power,'' which is proportional to voltage squared, is proportional to Eq. (1).] In Fig. 2, we compare the theoretical objective lens optical sectioning dictated by Eq. (1) with the optical sectioning realized by the Koester/Khanna interferometer with split-aperture objective.

The split aperture is made by placing an opaque vertical strip close to the back aperture of the objective lens (Koester *et al.*, 1994). The optical system is arranged so that the illumination beam uses one half of the lens and the reflected light uses the other half. Figure 2 shows that without the split aperture, the theoretical optical sectioning curve initially

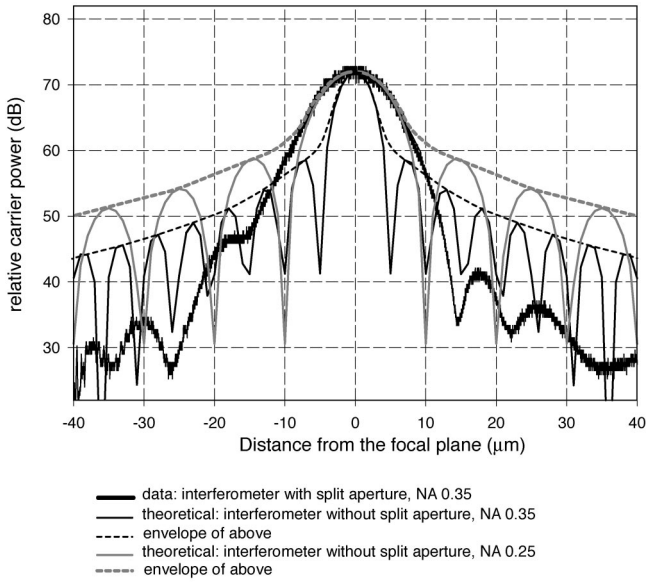

FIG. 2. Optical sectioning curve as a function of the distance of the reflector from the focal plane. The optical sectioning curve was measured by the carrier power in the heterodyne interferometer signal. We show: (i) Measured optical sectioning curve with split-aperture objective (NA=0.35, thick black line). (ii) Calculated optical sectioning curve due to objective lens without split aperture (NA=0.35, solid black line). (iii) Corresponding envelope (dashed black line). (iv) Calculated optical sectioning curve due to objective lens without split aperture (NA=0.25, solid gray line). (v) Corresponding envelope (dashed gray line). Near the focal plane ($d \leqslant \pm 10\ \mu$m) the optical sectioning curve of the split-aperture lens (NA=0.35) matches the theoretical curve for NA=0.25. This is because the split aperture reduces the effective aperture of the lens. However, away from the focal plane ($d \geqslant \pm 10\ \mu$m) the rejection of the split-aperture system is greater than that of the other systems.

falls off smoothly with distance but then rebounds due to diffraction sidelobes. It is the envelope of the curve that is relevant in practice, and therefore the envelopes of the theoretical curves have been included in our Fig. 2. The opaque strip in the split-aperture system provides steep fall-off away from the focal plane. The experimental curve shown in Fig. 2 does not represent a theoretical limit, and improvements of the split-aperture system are expected to extend the steep fall-off even further. A disadvantage of the split aperture is that the effective numerical aperture of the lens is reduced in one dimension. Thus, in the region of the peak (where the N.A. governs the curve shape) the data are very close to the theoretical results for a lens with N.A. 0.25, although the N.A. of the lens when fully illuminated is 0.35. The split-aperture arrangement offers substantial and increasing improvement in sectioning when the defocusing distance is greater than 10–15 μm. Table I compares the optical sectioning properties obtained with the split-aperture arrangement of Khanna *et al.* with that of several other interferometers.

B. FM interferometry

1. The demodulation process

a. Theory. In heterodyne interferometry a laser beam is divided into two beams: object beam (frequency f_o) and reference beam (frequency f_r). One or both beams are frequency shifted so that the frequency difference ($f_o - f_r$) between the two beams is f_c (carrier frequency). In our case

TABLE I. First column: (i) Paper from which the data are quoted. (ii) Magnification and numerical aperture (NA) of the objective lens used. (iii) Full width at half maximum (FWHM), the distance in μm between the two points where the carrier level drops to half power. Columns 2–5: distances from the focal plane in μm where the carrier power drops by factors of 10, 100, 1000, and 10 000, respectively. Symbol $\cdots$ indicates that the level was not reported.

Carrier power/maximum light rejection	10^{-1}	10^{-2}	10^{-3}	10^{-4}
Ren & Nuttall, 2001 20 X, NA 0.42 FWHM=19.5 μm	± 25	$\cdots$	$\cdots$	$\cdots$
Dalhoff *et al.*, 2001 (using the short coherence length laser diode) NA 0.14 FWHM=27 μm	$-28, +26$	$-44, +41$	$-60, +51$	$-75, +63$
Cooper, 1999a 5 X, NA 0.13 FWHM=75 μm (with respect to carrier power)	$-82, +65$	$-146, +156$	$\cdots$	$\cdots$
10 X, NA 0.25 FWHM=16 μm (with respect to carrier power)	$-16, +16$	$-40, +35$	$-83, +97$	$-272, +265$
Khanna *et al.*, 1996 20 X, NA 0.53 FWHM=4.2 μm	$-5, +3$	$-11, +4$	$-16, +10$	$-40, +20$
Figure 2 data above 20 X, NA 0.35 Nikon lens in air FWHM=9 μm	$-9, +8$	$-13, +12$	$-21, +13$	$-33, +30$

$f_o - f_r = 455$ kHz. The object beam is focused on the surface to be measured (for example, **A** in Fig. 1). The object beam reflects from the surface and is combined with the reference beam. The photodetector measures light power—the sum of the object and reference waves, quantity squared. When the sum is squared a term at the difference frequency, $f_o - f_r$, is produced (along with terms at the frequencies $2f_o$, $2f_r$ and $f_o + f_r$). f_r and f_o are too high in frequency to be resolved by the photodetector, and the photodetector's ac voltage output is at the difference frequency ($f_c = f_o - f_r$). The amplitude of this ac signal is proportional to the product of the reference and object wave amplitudes, or equivalently, to the product of the square root of the reference and object beam powers. (See Willemin *et al.*, 1988 and Cooper, 1999a for more details.) When the object (**A**) is moving, f_o is changing in time due to the Doppler shift, and $f_o(t) - f_r = f_c + f(t)$, resulting in the frequency-modulated (FM) signal $x_A(t)$

$$x_A(t) = a\cos\left(2\pi\int (f_o(t') - f_r)dt'\right)$$
$$= a\cos\left(\omega_c t + 2\pi\int f(t')dt'\right), \quad (2)$$

where $x_A(t)$ is the voltage input to an FM demodulator tuned to 455 kHz. Demodulation is accomplished by detecting the phase of the signal, $(\omega_c t + 2\pi\int f(t')dt')$, taking the time derivative to find the instantaneous frequency and subtracting the carrier frequency. For an unchallenged signal, this results in a perfect extraction of $f(t)$. Further along we will consider the effect of applying this simple algorithm to a signal that is challenged by the signal from a secondary object.

When the modulating signal is sinusoidal, $f(t) = \Delta f \sin(\omega_m t + \phi_A)$, the FM signal can be written as

$$x_A(t) = a\cos(\omega_c t - \beta\cos(\omega_m t + \phi_A))$$
$$\text{with} \quad \beta = \frac{2\pi\Delta f}{\omega_m}, \quad (3)$$

where f_m is the modulation frequency and corresponds to the frequency of the object's motion ($\omega = 2\pi f$). ϕ_A is the phase of the object's movement. Δf is the frequency deviation and is directly related to the velocity amplitude, V_o, as $\Delta f = 2V_o/\lambda$, where λ is the laser wavelength. This is the Doppler shift. β, the modulation index, can be expressed as a function of velocity amplitude ($\beta = 2V_o/\lambda f_m$) or displacement amplitude ($\beta = 4\pi X_o/\lambda$).

The spectrum of x_A can be expressed in terms of Bessel's functions $J_n(\beta)$. It contains a carrier component and an infinite set of sidebands located symmetrically on either side of the carrier ($f_c \pm nf_m$). For small modulation index, only the Bessel's coefficients $J_0(\beta)$ and $J_1(\beta)$ have significant values, so that the FM signal is effectively composed of a carrier and a single pair of sidebands at $f_c \pm f_m$.

First, consider the velocity of a single surface. At what defocus value would the demodulator fail to accurately report the velocity? The ability to measure vibration depends on the carrier to noise ratio (C/N) at the input of the demodulator. In the most sensitive detection method, the noise level at the photodetector output is determined by the shot noise N, which is directly proportional to the reference beam power. (The reference beam is made powerful enough so that this condition obtains.) For the FM demodulator to function the C/N must exceed 10 dB with the full 150-kHz bandwidth of the demodulator (Willemin *et al.*, 1988). This is known as the ''threshold effect'' in the FM literature (Panter, 1965). As the surface is moved away from the focal plane the light in the object beam will decrease, and so the carrier power will

decrease while the shot noise will remain constant. As long as the carrier power remains at least 10 dB above the noise power, the demodulator will continue to measure the vibration of the object. For example, when measuring from a naturally bright reflector such as guinea pig Hensen's cell, the maximum carrier power in our system is -10 to -20 dB. Shot noise is -68 dB. With a 0.35 numerical aperture objective lens, the optical sectioning of the split-aperture system (Fig. 2) will decrease the carrier signal to -58 dB at a distance of $\sim +/-25$ μm from the focal plane. Because the FWHM of the optical sectioning curve with this lens is only ~ 9 μm, the recording depth—the defocus value for which the velocity is accurately reported—can be broader than the FWHM. This is the same effect that was discussed by Ren and Nuttall (2001). The defocus distance over which the vibration can be measured depends on the interferometer optical sectioning, the incident light power, and the reflectivity of the surface. The steeper the optical sectioning, the narrower will be the allowed defocus distance. Lower incident light and lower reflectivity also narrow the allowed defocus distance. In summary, the relatively broad allowed defocusing distance can be understood in terms of the FM demodulator's threshold C/N ratio.

The relatively large defocus distance over which velocity can be measured accurately will not influence the result when measuring the motion of a single surface. However, the observation does raise questions about the effect a secondary surface, which is within the allowed defocus distance of a primary surface, would have on a measurement of the primary surface's motion. In brief, when measuring through multiple surfaces, it is important that the interferometer measures the vibration of the surface that is in focus. This depends both on the optical sectioning and how the demodulator responds to competing signals. The optical sectioning determines how much the competing signal is reduced, and the demodulator determines how much the residual competing signal affects the measurements.

Therefore, we take up the question of competing signals. Returning to Fig. 1, assume that point **A** moves with velocity $V_A(t)$ upon sound stimulation, and point **C** on the lamina moves with velocity $V_C(t)$. If **A** is at the focal plane, light reaching the detector from surface **C** will be attenuated according to the optical sectioning characteristics of the interferometer. How will the signal from **C** influence the reported velocity? The photodetector output will contain an ac component from the interference of the **A** wave and the reference wave: $x_A(t)=a\cos(\omega_{cA}t-\beta_A\cos(\omega_m t))$. The photodetector output will also contain an ac component from the interference of the **C** wave and the reference wave: $x_C(t)=c\cos(\omega_{cC}t-\beta_C\cos(\omega_m t+\phi_C)+\psi_0)$. The amplitudes c and a are proportional to the square root of the light power in the **C** and **A** waves. ϕ_C represents the phase of the movement at **C** relative to at **A**. ψ_0 is the relative phase between the **A** and **C** light waves, due to the optical path length difference. ψ_0 depends on the distance at rest between the two surfaces. In order to reduce the number of parameters we will only treat the case $\phi_C=0$. $\omega_{cC}=\omega_{cA}=\omega_c$, but we write them with different symbols to discuss signal competition more generally. For example, ω_{cC} not equal but close to ω_{cA} is the situation with two competing FM radio signals. There will be a third ac component due to interference of the **A** and **C** waves with each other, but its frequency will be far from the carrier frequency the FM demodulator is tuned to and will not influence the demodulation. Therefore, the relevant ac voltage at the demodulator will be $x(t)=x_A(t)+x_C(t)$. The mathematics involved in adding the two signals is just like that used to discuss "beats" in the general case in which the two signals that make up the beat are not of equal amplitude. Using phasor algebra, $x(t)$ is written as

$$x(t)=a[\sqrt{1+\rho^2+2\rho\cos(\varphi)}]\cos(\omega_{cA}t-\beta_A\cos(\omega_m t)+\theta),$$

$$\text{with}\quad \rho=\frac{c}{a};\quad \varphi=(\omega_{cC}-\omega_{cA})t+\psi_0-(\beta_C-\beta_A)\cos(\omega_m t),$$

$$\text{and}\quad \tan(\theta)=\frac{\rho\sin(\varphi)}{1+\rho\cos(\varphi)}. \tag{4}$$

The amplitude of the signal $x(t)$, $a\sqrt{1+\rho^2+2\rho\cos(\varphi)}$, is modulated. To a first approximation, this will not affect the output of the FM receiver. Indeed, during the demodulation process, the signal $x(t)$ is clipped in order to remove any amplitude modulation. This clipping is performed by the "limiter."

The demodulation process consists of the extraction of the instantaneous frequency, $\omega_i(t)\equiv d\psi/dt$, from the phase, $\psi(t)=(\omega_{cA}t-\beta_A\cos(\omega_m t)+\theta)$. Finally, the carrier frequency is subtracted to give the demodulated output signal, $E(t)$

$$E(t)=\omega_i(t)-\omega_{cA}=2\pi\Delta f_A\sin(\omega_m t)+\frac{d\theta}{dt},$$

$$\text{with}\quad \theta=\arctan\left(\frac{\rho\sin(\varphi)}{1+\rho\cos(\varphi)}\right),\quad \rho=\frac{c}{a},$$

$$\varphi=(\omega_{cC}-\omega_{cA})t+\psi_0-(\beta_C-\beta_A)\cos(\omega_m t). \tag{5}$$

[A generalization of Eq. (5) for which $\phi_C\neq 0$ is included in a footnote.[1]] Equation (5) is useful to study the theoretical influence of a competing signal $x_C(t)$ on the output of the FM receiver. The first term gives the output in the absence of the competing signal. The second term shows the effect of competing signals. This "error" in the instantaneous frequency depends on the modulation indices β_C, β_A, on the ratio ρ of the amplitudes of the secondary and primary signals, on their relative phase ψ_0, and on the difference of their carrier frequencies. The time derivative of the angle θ in Eq. (5) can be calculated directly by using MATLAB. Alternatively, an expansion of this term in Bessel's functions is presented by Panter (1965). When $\omega_{cC}\neq\omega_{cA}$ (as for two competing radio stations) the relative phase between the two signals changes with time and the value of the phase ψ_0 doesn't matter—it can be neglected. When both carrier frequencies are the same, as for optical interferometry, the phase ψ_0 depends on the distance between the two surfaces without stimulation and is an important parameter.

In practice, FM receivers include a cascade of nonideal limiters and bandpass filters. In contrast, the theoretical expression Eq. (5) corresponds to an ideal limiter without filter. The cascade of limiters and filters was developed in part to

reduce the effect of competing signals and, in addition to Eq. (5), a computer model has been developed that probes the effect of the cascade.

b. How the FM receiver works—Principle of the model. One step of the FM receiver is to shift the carrier frequency to an intermediate frequency (11 MHz, IF bandwidth $=150$ kHz for our receiver). Then, the signal goes through a limiter: An ideal limiter clips the signal in order to eliminate any amplitude variations. Due to the limiting process, the spectral components of the signal are spread out. A bandpass filter following the limiter passes spectral components centered about the carrier frequency and removes their harmonics. The bandwidth of the bandpass filter is the IF bandwidth. Baghdady (1956, 1961) discusses the competing signal problem, and how the size of the bandwidth should depend on the ratio of signal strengths. The limiter bandwidth must be wide enough to pass a sufficient number of sideband components to add up to a resultant signal whose average frequency at the input of the discriminator is equal to the frequency of the stronger of the two competing signals. During the process of amplitude limiting followed by a filtering, a reduction of the effective amplitude of the competing signal is achieved. For more details see Middleton (1981, 1996). The way we implemented the computer-model FM demodulator was as follows: We started with the signal $x(t)$, clipped it to retain only the zero-crossing times, and then bandpass filtered it. The filter was a window applied in the frequency domain with a bandwidth of 150 kHz. The clipping and filtering was repeated five times. Finally, the instantaneous frequency was found with the zero-crossing times of the processed signal. [Zero crossings were found with software; the way that an electronic circuit figures zero-crossing times was described in Cooper (1999a).] Our objective with this simple model was to demonstrate the basic method by which FM demodulator electronics can reduce the effect of competing signals beyond what Eq. (5) predicts, and for that it was useful.

c. Realistic parameter values. Before delving into the analysis of Eq. (5), it is useful to consider the β, X_o, and ρ values that normally occur in an intracochlear measurement. The division between high- and low-modulation index is at a β value of $\sim 0.5-2$, corresponding to displacements, $X_0 = 25-100$ nm (using a He–Ne-like diode laser, $\lambda = 638$ nm). The measured range of displacement depends on cochlear position (apical vs basal), the structure considered (basilar membrane, Hensen's cell), and on species. For basal basilar-membrane (b.m.) measurements in chinchillas, X_o extends from 0.1 to 200 nm. For guinea pigs, basal b.m. displacements range from 0.05–40 nm. For tectorial membrane measurements in chinchillas, the measured displacements extend from 0.7 to 200 nm [e.g., the reviews of Robles and Ruggero (2001) and Ulfendahl (1997)]. For apical b.m. measurements in guinea pigs, the displacement extends from 6 to 36 nm (Khanna, 1998). Clearly, the intracochlear measurements extend into both high and low modulation cases.

$\rho = c/a$ is the ratio of signal coming from the secondary surface (**C**) to signal coming from the primary surface (**A**). To be precise, the signal strength (carrier level of the interferometer signal) from an object in the cochlea depends on several quantities: the object's reflectivity, R; the object's relative interference amplitude, m [m represents wavefront distortion and takes values less than 1 (Khanna *et al.*, 1996)]; on the distance between the object and the plane of focus (d), and the value (k) the carrier power takes at this distance due to the optical sectioning. R, m, and d depend on the cochlea and k depends on the interferometer optics. The heterodyne signal power from the surface **A** will be proportional to ($m_A^2 R_A k_A$) and the heterodyne signal voltage (a from the above) to $\sqrt{m_A^2 R_A k_A}$. Finally, the ratio $\rho = c/a$ is found by taking the ratio of signal voltages from two surfaces. Consider the following example, in which the motion of the organ of Corti is probed in guinea pig from the scala vestibuli side. Physiologically it is an interesting approach as measurements of several key cochlear structures—Hensen's cells, hair cells, and basilar membrane, can be made (Khanna and Hao, 2000). In order to measure basilar-membrane motion from scala vestibuli adjacent to the Hensen's border region, the incident laser beam passes through the Reissner's membrane, through Claudius's cells, and is focused on the b.m. (Khanna and Hao, 2000). For the b.m., which is in focus, $k=1$. The reflectivities and relative interference amplitudes of the b.m. in the tunnel region, outer hair cells, Hensen's cells, and Reissner's membrane were measured with an apical turn approach, and the values reported in Khanna *et al.* (1996).

The values in the table below are from that reference. In guinea pig, Hensen's cells are quite reflective due the lipid droplets they contain. The relative sizes of the signal from the target (basilar membrane) and the competitors (Reissner's membrane or Hensen's cells) are found by comparing $\sqrt{m^2 R k}$ for the three. The ratio of the $\sqrt{m^2 R k}$ values gives ρ. The relative interference amplitude (m) depends on the state of focusing. The representative m value of a tissue is found with the surface in focus. When the surface is out of focus, the m value might change because the tissue surface is not flat. The change in m with defocus has not been measured, and m is treated as a constant in Table II. Therefore, the ρ values listed and competition indicated are upper bounds. This ratio, listed in the final column of Table II, will guide the interpretation of the studies on competing signals below. In this example the reflective Hensen's cells, with a ρ value that varies between 0.06 and 0.13, pose the most serious challenge to a measurement of b.m. motion from scala vestibuli.

In summary, both low and high β are found in intracochlear motion measurements. Regarding ρ, most major surfaces in the cochlea are separated by at least 100 μm. With this separation, in the special case of two surfaces with equal reflectivity, the ρ values are less than 0.1 for all the systems in Table I. When the surfaces do not have equal reflectivity, steep optical sectioning is needed to reduce ρ, as the example above makes clear. As cochlear measurements begin to probe motion at the cellular level, steep optical sectioning becomes even more essential.

d. Numerical results. In this section the ideal demodulation described by Eq. (5) and the demodulator cascade model are used to study the influence of β_C, β_A, ρ, and ψ_0 on $E(t)$. Results obtained with both methods are compared. We only show results for the case in which $\omega_{cC} = \omega_{cA} = \omega_c$ be-

TABLE II. Calculation of relative signals from b.m, r.m. and H.C. when laser beam is focused on the b.m. d = distance from b.m., k = optical sectioning factor, R = reflectivity, m = wavefront distortion factor, m^2Rk = relative carrier power, ρ = square root of the ratio of carrier power of out-of-focus structure to carrier power of in-focus b.m.

	d	k	$R\times10^{-5}$	m	$m^2Rk\times10^{-7}$	ρ
Basilar membrane	0	1	2.1	0.14	4	
Reissner's membrane	$\sim$290 μm	10^{-4}	3.5	0.13	0.0006	0.012
Hensen's cells (lipid droplets) shoulder region	$\sim$60 μm	10^{-4}	38–89	0.19–0.28	0.014–0.07	0.06–0.13

cause this applies in heterodyne interferometry. We studied in depth the case in which the competing surface was stationary: $\beta_C=0$ and $\beta_A\neq0$. This corresponds to the experimental condition of Fig. 1, in which the stationary, highly reflective bone is the competing signal. We also considered the case that corresponds to the primary surface stationary and the secondary surface moving: $\beta_C\neq0$, $\beta_A=0$. Results from this case can be used to understand the interference that arises when a competing surface moves much more than the in-focus surface.

Figure 3 shows $E(t)$ using Eq. (5) (ideal limiter without filter) for both low and high modulation index (upper curve: $\beta_A=0.2$; lower curve: $\beta_A=4$; $\beta_C=0$ for both curves). Results without competing signal (thin line: $\rho=0$) are compared to those with competition (thick and dashed curves: $\rho=0.6$ and $\psi_0=0$ deg). Based on the section above, the ratio used for this plot is much larger than what would normally occur in the cochlear experiments; the purpose of the plot is to clearly illustrate the differing effects of a competing signal when the modulation index of the primary signal was low compared to when it was high. At low modulation index the output signal was reduced in size but undistorted. The high-modulation-index signal was distorted but the amplitude of the fundamental frequency was unchanged. The dashed curves in Fig. 3 illustrate the effect of the FM demodulator cascade. The cascade of limiters and filters produced no change for the low-modulation-index case (the dashed curve is superimposed on the thick one), whereas at high modulation index the distortion in the time domain was reduced. The characteristics of the spectrum of an FM signal are helpful to explain this observation: The limiter, which spreads the components of the spectrum, has more effect at high modulation index, where the spectrum contains a carrier component and an infinite set of sidebands, compared to the low-modulation case, where the significant components are at $f_c\pm f_m$. The filter removes more sidebands for the high-modulation-index case.

Figure 3 showed the influence of a competing signal on $E(t)$ in the time domain. In Fig. 4 we look at the same results in the frequency domain, and consider the amplitude of $E(t)$ at the stimulus frequency, f_m. Difference in the amplitude of $E(t)$ at frequency f_m is compared to the case without a competing signal (where $\rho=0$). The result is shown as a function of the ratio ρ for different values of phase, ψ_0. Figure 4(A) shows the effect of an unmodulated signal ($\beta_C=0$) of amplitude c on a low-modulation-index signal ($\beta_A=0.2$). The modulation frequency was 9.6 kHz. This panel illustrates the strong dependence of the output on the relative phase between competing signals. When the phase between the signals was equal to 0 deg, the output decreased as the

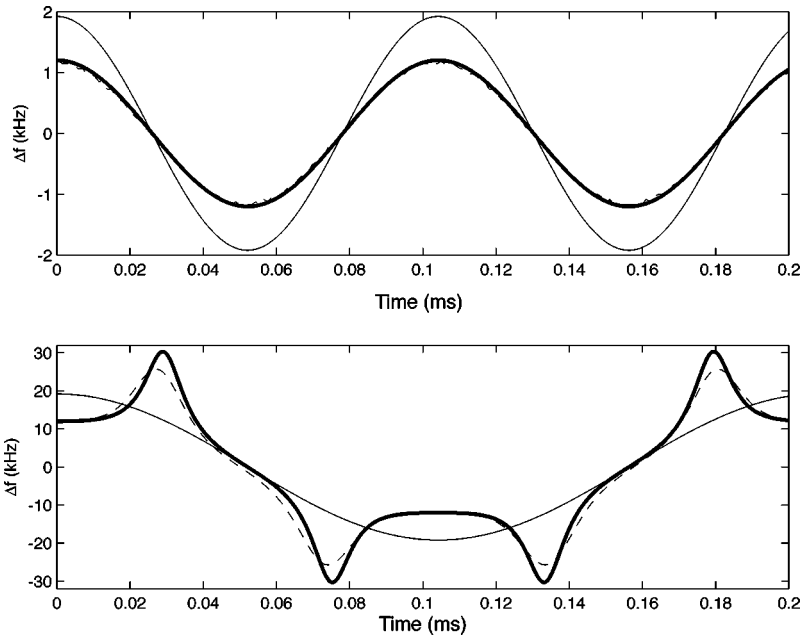

FIG. 3. Comparison of calculated results using Eq. (5) (thin and thick lines) with simulated model FM receiver results (dashed line), with and without a competing signal. The top panel shows demodulator output for low modulation index ($\beta_A=0.2$, $f_m=9.6$ kHz, $\Delta f=1.92$ kHz, $\psi_0=0$ deg), while the bottom panel shows results for high modulation index ($\beta_A=4$, $f_m=4.8$ kHz, $\Delta f=19.2$ kHz, $\psi_0=0$ deg). The thin line on both panels shows output without competition ($\rho=0$). Thick and dashed lines on both panels show demodulator output with competition ($\rho=0.6$). For low modulation index (top), a strong competing signal reduces the amplitude of the output by 4 dB, but the waveform remains unchanged. The results using Eq. (5) are very close to those obtained with the simulated FM receiver. For high modulation index (bottom), the time waveform is distorted by the strong competing signal. The results from Eq. (5) are close to those obtained by simulated FM receiver. The distortion predicted by the latter is slightly lower.

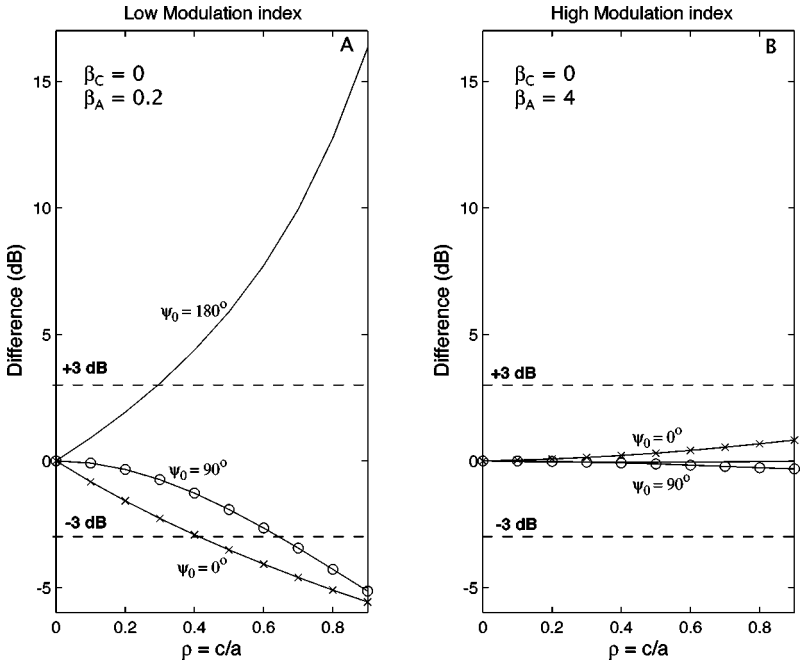

FIG. 4. Changes in the demodulator output amplitude due to the presence of a competing signal as a function of the ratio ($\rho = c/a$) and for different values of phase ψ_0: (x) 0 deg; (o) 90 deg; and (-) 180 deg. Panel (A), low modulation index of 0.2 ($\beta_A = 0.2$, $\beta_C = 0$, $f_m = 9.6$ kHz). Demodulator output can decrease or increase substantially depending on the relative phase of the two competing signals and their relative amplitudes. The worst case is when the two signals are 180 deg out of phase. Panel (B), high modulation index of 4 ($\beta_A = 4$, $\beta_C = 0$, $f_m = 4.8$ kHz). The demodulator output at the stimulus frequency remains substantially unchanged even in the presence of a strong competing carrier.

ratio increased (as the relative size of the unmodulated signal increased). When the ratio was equal to 0.9, a decrease of 5 dB was observed. This result suggests that in the low-modulation-index case the effect of a competing signal can be thought of in terms of a weighted average: The output is approximately equal to the amplitude (strength) of each signal (a or c) multiplied by its own frequency deviation (which in the case of the cochlear experiments is proportional to the velocity, and in the case at hand was zero for signal **C**), and divided by $(a+c)$. An expansion of Eq. (5) for $\beta \ll 1$ confirms this. When the phase between the signals was equal to 180 deg the weighted average idea still applies, except the divisor is equal to $(a-c)$, which produces the observed *increase* in output. The result highlights the strong effect of the phase. In terms of an optical experiment, 180 deg phase will occur when twice the distance between the two surfaces is $(n+\frac{1}{2})\,\lambda$, where n is an integer. The 0 deg phase will occur when twice the distance between the two surfaces is $n\lambda$. With $\psi_0 = 0$ deg, to have an error on the output less than $+/-3$ dB, the ratio of the interfering signal over the modulated signal needed to be less than 0.4 and, when $\psi_0 = 180$ deg, this value was smaller, 0.3. ψ_0 of 0 and 180 deg were worst cases, and intermediate phases showed smaller errors. In general, harmonic distortion was small for low modulation index: For $\beta_A < 0.5$, with a ratio of 0.4 or less, the amplitude of harmonic components was at least 30 dB down (with $\beta_A = 0.2$, $\beta_C = 0$, $\psi_0 = 90$ deg) compared to the fundamental (not shown).

Figure 4(B) shows the change in $E(t)$ with ρ at the frequency f_m due to a competing signal in the high-modulation-index case ($\beta_A = 4$, $\beta_C = 0$, $f_m = 4.8$ kHz). Changes in the output at the stimulus frequency were less than 1 dB for all ratios and phases. However, as shown in Fig. 3, the output was distorted in the time domain. In order to have the harmonic components at least 25 dB down, the ratio needed to be less than 0.1 (not shown). Based on the ρ values in Table II, even with steep optical sectioning a detection of distortion must be treated with caution when competition from secondary signals is a possibility and displacements are relatively large.

To summarize the theoretical section in the case of $\beta_C = 0$: The theoretical effect of competing signals at the input of the receiver was described first in the time domain. At low modulation index, there was a change of the amplitude of the signal but it was not distorted. The design of the receiver (cascade of limiters and filters) did not reduce the effect of a competing signal. At high modulation index the competing signal produced distortion in the output that could be reduced by the processing of the FM receiver. In the frequency domain the theoretical influence of a competing signal on the receiver output at the fundamental frequency was shown in Fig. 4. For low modulation index, an increase or decrease of the output was found, depending on the relative phase of the two signals. The simple notion of a weighted average gave a reasonable estimate of the effect of competing signals. At high modulation index, with respect to the amplitude of the fundamental component the output error was always less than 1 dB, even when the competing signals were nearly equal [Fig. 4(B)]. However, the theoretical output waveform was distorted in the presence of the competing signal.

We began with the case $\beta_C = 0$ and $\beta_A \neq 0$. Equation (5) is now used to explore the opposite case, $\beta_C \neq 0$ and $\beta_A = 0$. When the input is the unchallenged signal **A**, the output is zero. The time-domain plots in Fig. 5 show the effect of either low-modulation (left column) or high-modulation (right column) competing signal **C**. The top panel in each column shows the frequency deviation of the competing signal **C**—the output if signal **C** was the sole input. The middle and bottom panels show the effect of this competing signal when it is combined with signal **A** ($\beta_A = 0$) at ratios of 0.3 and 0.05. The low-modulation/high-modulation classification of results found above still applies. The low-modulation competitor leads to an undistorted, but nonzero output that is like the output for the competing signal **C** alone shown in the

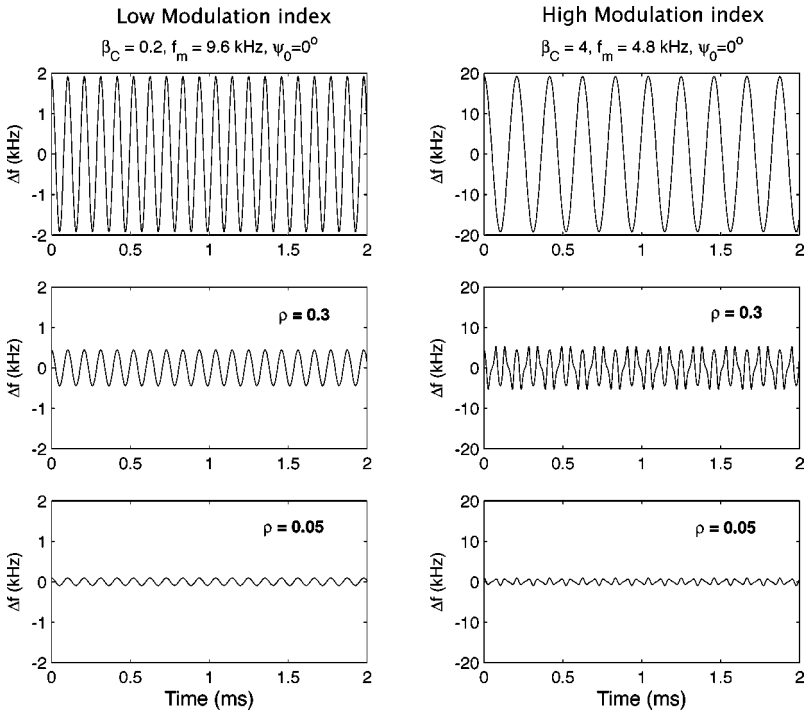

FIG. 5. Results calculated from Eq. (5) with $\psi_0 = 0$ deg. This experiment simulates the influence of a vibrating surface when the interferometer is focused on a stationary surface ($\beta_A = 0$). The unmodulated carrier is larger than the competing modulated carrier signal. The upper curves correspond to the competing signal itself ($a = 0$). The middle and lower panels show the effect of a modulated signal combined with signal **A** ($\beta_A = 0$, $\beta_C \neq 0$) for a ratio ($\rho = c/a$) of 0.3 and 0.05. For the low modulation index ($\beta_C = 0.2$, left column) even when the competition is weak (0.05) the demodulator output contains a modulation component. For the high modulation index case ($\beta_C = 4$, right column) the demodulator output is highly distorted.

top panel but with a substantially reduced amplitude. This is as expected since the unmodulated signal **A** is stronger than **C**. The size of the output scales with ρ, the relative strength of competing signal **C**, and as above, a weighted-average rule of thumb applies for the low-modulation case. The high-modulation competitor leads to a highly distorted output. The distorted output has odd symmetry and possesses only odd harmonics because it was calculated with ψ_0 equal to zero; in general, the output is composed of both even and odd harmonics.

2. Electronic experiments with two generators

To simulate competing signals, x_A and x_C were generated with two signal generators. Again, we begin with the case $\beta_A \neq 0$, $\beta_C = 0$. The first generator produced a frequency-modulated signal with a carrier frequency 455 kHz, corresponding to interference between the reference beam and **A** ($x_A(t) = a\cos(\omega_{cA}t - \beta_A \cos(\omega_m t))$). The second signal generator produced a signal at 455 kHz with no frequency modulation, corresponding to interference between the reference beam and **C** ($x_C(t) = c\cos(\omega_{cC}t)$). To test the above theoretical results, the sum $x(t) = x_A + x_C$ was frequency shifted to 100 MHz and then applied at the input of our demodulator and the output was measured. (The shift in frequency is a processing detail that is not important to the message of this paper.) Although both signal generators were set with $f_c = 455$ kHz, in fact the two generators were not phase locked and their carrier frequencies were slightly different. They were close in frequency, so the resulting sum can be thought of as the sum of two signals with the same carrier frequency and a slowly varying relative phase ($\omega_{cC}t = (\omega_{cA} + d\omega)t = \omega_{cA}t + \psi_0(t)$). Thus, the experimental setup could be compared to the theoretical situation of Eq. (5) with $\omega_{cC} = \omega_{cA}$ and ψ_0 slowly varying. As ψ_0 varied slowly from 0 to 180 deg to 360 deg, the effects of the phase were compared with the predictions of Fig. 4. f_m and Δf were chosen to represent different values of the modulation index ($0.04 < \beta < 4$). f_m values were 4.8 and 9.6 kHz and Δf was from 200 to 38 000 Hz (so that in terms of a cochlear experiment, the velocity amplitude "V_o" was 0.06–12 mm/s and the displacement amplitude "X_o" was 2–200 nm). The output of the FM demodulator, $E_g(t)$ (the subscript g designates the generator experiments) was measured first with just signal **A**, and then as the level of signal **C** was increased (increase of the ratio ρ). For each ratio, $E_g(t)$ was measured and stored. The amplitude of $E_g(t)$ at the modulation frequency f_m was determined by Fourier transform (FT). The FT was performed over a portion of $E_g(t)$ where the two signals were in phase ($\psi_0 = 0$ deg) and out of phase ($\psi_0 = 180$ deg), as well as over the whole signal.

The upper curve of Fig. 6 shows $E_g(t)$ as a function of time ($\beta_A = 0.2$, $f_m = 9.6$ kHz, $\rho = 0.6$). (Note that this ratio is much larger than what is expected to occur in cochlear measurements. As above, the large ratio is used for illustrative purposes.) The signal in the time domain contained regularly spaced peaks. We could interpret these peaks in terms of the time-varying relative phase, ψ_0. At the time of the maxima in $E_g(t)$, the input signals were out of phase and at the time of the minima, the signals were in phase. The time between two maxima was the period of the frequency difference, $1/(f_{cC} - f_{cA})$. The lower curve of Fig. 6 is a zoom on a small portion (0.2 ms) of the upper curve, at a time when x_A and x_C were in phase. The theoretical output was calculated using Eq. (5) (dashed line; lower curve Fig. 6) and compared to the experimental one (solid line). The two figures agreed well, indicating that $E(t)$ resulting from the theory was useful to predict the receiver output, $E_g(t)$.

Figure 7 shows a high-modulation-index case. $E_g(t)$ is shown as a function of time as the bold curve ($\beta_A = 4$, $f_m = 4.8$ kHz, $\rho = 0.6$). The 1-ms periodicity is due to the time-

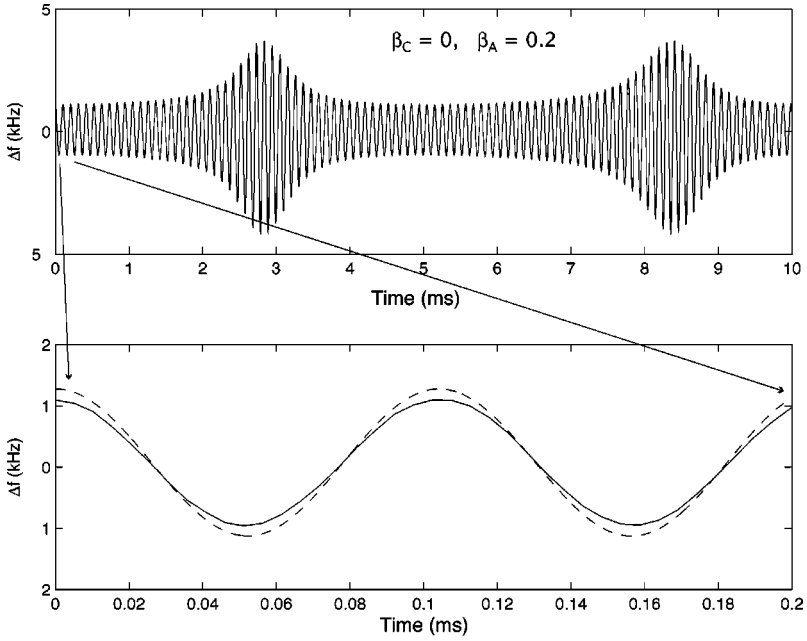

FIG. 6. Upper curve: Experimental output of the FM receiver as a function of time ($\beta_A=0.2$, $\beta_C=0$, $f_m=9.6$ kHz, $\rho=0.6$). Lower curve: superposition of the theoretical instantaneous frequency (dashed line) and the experimental one (solid line) over a short period of time. The generators producing the FM and the competing signals were not phase locked. Their relative phase changed with time and, as a consequence, the demodulator output amplitude fluctuated with time increasing to a peak when the phase difference was 180 deg, and decreasing to a minimum when the phase angle was 0 deg [see Fig. 4(A)].

varying relative phase between the primary and secondary input signals. We include two other curves for comparison. The dashed curve shows the unchallenged output due to signal **A** (when signal **C** was off). The bold curve is distorted relative to the unchallenged signal. During the course of the measurement, the relative phase between the two signals, changes and this is reflected in the changing wave shape of the bold curve. Its overall size does not change. The thinner curve shows the predicted effect of the competing signal using Eq. (5). It is slightly more distorted than the output of the demodulator, confirming that the actual workings of the FM demodulator reduce the effect of competing signals in the high-modulation-index case.

Figure 8 presents an analysis of experimental data like that of Figs. 6 and 7 for a wide range of ratio ρ. In Fig. 8, the change in $E_g(t)$ (amplitude at f_m) due to a secondary signal compared to $E_g(t)$ without competing signal ($\rho=0$) is shown as a function of the ratio ρ. For each of the curves, the Fourier transform is performed in a different part of the time domain of a curve like Fig. 6, which allows us to infer the influence of the phase. Panel (A) corresponds to the low-modulation-index case (analysis of experimental data like that of Fig. 6). When the Fourier transform is performed in the part of the time domain where $E_g(t)$ is peaked at a maximum, corresponding to $\psi_0=180$ deg (plain curve), the competing signal caused an increase in the receiver output of 7 dB for a ratio of 0.6. When the FT was done where $E_g(t)$ was minimum, corresponding to $\psi_0=0$ deg (curve with crosses), then there was a decrease of 4 dB for the same ratio of 0.6. Figure 8(A) can be compared to the theoretical results shown in Fig. 4(A) (low modulation of $\beta_A=0.2$, $f_m=9.6$ kHz). They agree well. When the FT was done over

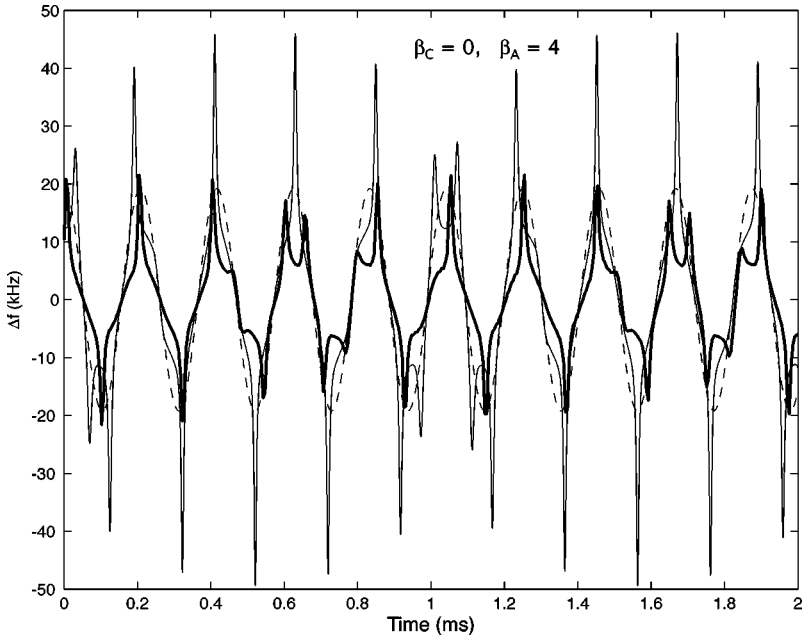

FIG. 7. Effect of a competing signal on the demodulator output (high modulation index: $\beta_A=4$, $\beta_C=0$, $f_m=4.8$ kHz, $\rho=0.6$). The bold curve was measured experimentally and is compared with calculated curves: The thin curve is the theoretical result using Eq. (5), whereas the dashed curve is the expected curve without competing signal. Both experimental and theoretical results show distortion of the sinusoidal waveform. The distortion in the experimental results is slightly less than that predicted by Eq. (5).

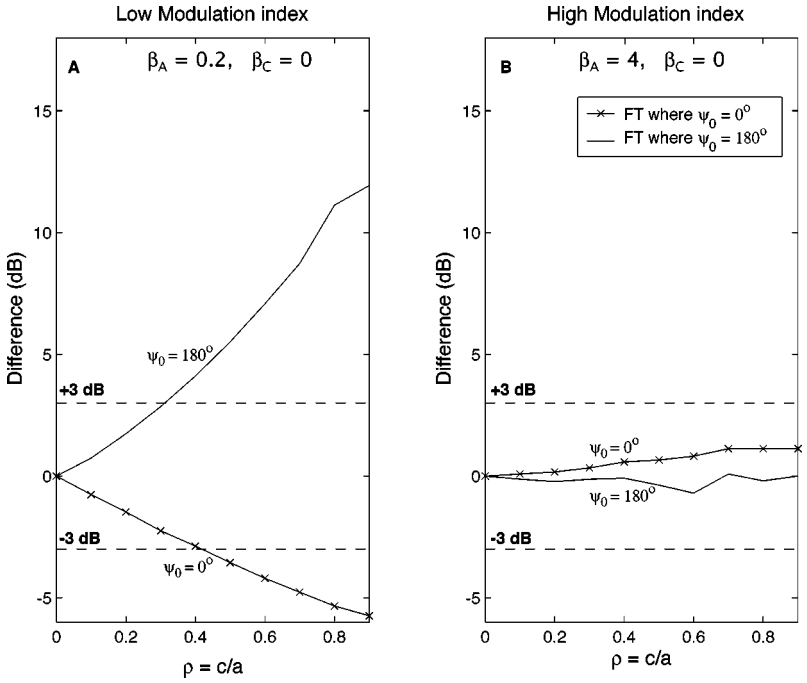

FIG. 8. Change in demodulator output (amplitude at f_m) with different magnitudes of competing carrier levels (ρ). Experiments were similar to those described in Figs. 6 and 7, but with ratio ρ ranging from 0 to 0.9. The values in the solid curve were derived from the peak region of the demodulator time varying output (where $\psi_0 = 180$ deg). Values in the curve with crosses were derived from the valley region of the curves (where $\psi_0 = 0$ deg). Panel (A) corresponds to the low-modulation-index case ($\beta_A = 0.2$, $\beta_C = 0$, $f_m = 9.6$ kHz) and panel (B) to the high-modulation-index case ($\beta_A = 4$, $\beta_C = 0$, $f_m = 4.8$ kHz). Results are similar to those predicted by theory (Fig. 4).

the entire signal, there was an average over the phase, and the output, even for a ratio of 0.9, was close to the output of the signal without competition (not shown). Therefore, when signals have different carrier frequencies, a time average can minimize the effect of competing signals. However, in the case of the interferometer, both secondary and primary signals have the same carrier frequency, and time averaging does not reduce the effect of competition.

Figure 8(B) presents an analysis of experimental data at large β ($\beta_A = 4$, $f_m = 4.8$ kHz). It illustrates the weak dependence of the amplitude at the stimulus frequency on the relative phase between carrier signals for the high-modulation-index case. The error is within +/-1 dB for all phases and ratios. Figure 8(B) can be compared to the theoretical results shown in Fig. 4(B). They agree well.

To summarize the experimental results with generated signals in the case $\beta_A \neq 0$, $\beta_C = 0$ (secondary signal not frequency modulated):

At low modulation index (β_A) when two signals with approximately the same carrier frequency were summed at the input of the receiver, and when they were in phase, the error due to the competing signal **C** produced a decrease of the demodulator output. When they were out of phase, the error produced an increase in the demodulator output. The FM demodulator output depended strongly on the ratio of the amplitude of both signals and their relative phase. The output waveform was not distorted by the competing signal.

For high modulation index (β_A), the output of an FM demodulator at the stimulus frequency was not influenced by the competing signal **C** even when the secondary signal was nearly as large as the primary signal. However, the output signal was distorted.

The most important conclusion from these results is that the theoretical expression for $E(t)$ in Eq. (5) was very useful for predicting the output of the FM demodulator, $E_g(t)$. In the high-modulation-index case, the distortion predicted by Eq. (5) is an upper bound, as the FM demodulator did offer some improvement in reducing distortion.

The study with signal generators and FM demodulator above concerned the case $\beta_C = 0$ and $\beta_A \neq 0$. The opposite case, $\beta_C \neq 0$ and $\beta_A = 0$, has also been explored. Curves similar to those of Fig. 5 were obtained (not shown). These results confirm the low-modulation/high-modulation classification of results that was noted already, and also confirm the usefulness of Eq. (5) for predicting the demodulation.

3. Optical experiments with the interferometer

Above we compared the theoretical predicted effect of competing FM signals to experimental results using generated FM signals and our REVOX FM demodulator. Below we complete the study by measuring the effect of competing signals that were produced by reflective surfaces, using the confocal-heterodyne interferometer developed by Khanna *et al.*, 1996. We explore first the case in which the secondary surface was fixed, $\beta_C = 0$, $\beta_A \neq 0$, and then the case in which both surfaces were moving, $\beta_A \neq 0$, $\beta_C \neq 0$. The setup is shown in Fig. 9. The system was composed of two surfaces: A glass tube with a semitransparent thin plastic membrane at its end was used as a vibrating object. It was fixed to a stiff steel rod. The back surface was a polished steel fiber, fixed rigidly to a micropositioner. The position of this fiber was adjusted by using a calibrated piezoelectric translator. Vibrations were measured for several separations of the front and back surfaces. The fiber was inserted at a distance as close as 22 μm from the front surface. The front surface was vibrated by driving it with a speaker at $\omega_m = 2\pi f_m$. The back surface was stiff and did not vibrate with the sound stimulation. The laser's object beam was focused at the center of the membrane. The primary signal, $x_A(t)$, was produced by interference between the object beam that reflected from the membrane and the reference beam. The secondary signal, $x_C(t)$,

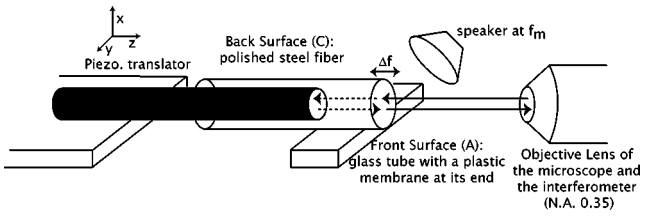

FIG. 9. The setup shown was used to optically simulate the multiple reflection conditions that might be encountered in the cochlea. A thin plastic membrane at the end of a glass tube (diameter= 1.2 mm) was used as one of the partially transmitting/reflecting surfaces. This membrane could be vibrated with the sound from a speaker placed near it. By changing the frequency and intensity of sound, the frequency and amplitude of membrane vibration could be controlled. The vibrating membrane produced the frequency-modulated component of the carrier. A polished surface of a steel fiber inserted in the tube provided the second reflecting surface. This surface was considered stationary and provided the unmodulated component of the carrier. Piezoelectric and mechanical translators allowed the steel fiber to be positioned precisely with respect to the plastic membrane. Mechanical translators in the interferometer were used to position the whole assembly together with respect to the objective lens. This allowed the position of the focal plane to be changed and measured with 1-μm resolution. Carrier level (measured using a spectrum analyzer) and demodulator output (proportional to the velocity) were measured as a function of distance from the front surface.

was produced by interference between the object beam reflected from the fixed back surface and the reference beam. The relative phase between the two signals was constant and depended on the distance (d) between the two surfaces without stimulation: $\psi_0 = 2d2\pi/\lambda$, with λ the laser wavelength. Measurements were made at different positions of the plane of focus: from 10 μm in front of the membrane to 10 μm behind the back surface. For each position, the carrier level and the demodulator output were measured.

First, the vibration of the membrane alone (front surface) was measured. The measured carrier level was always at least 30 dB above the shot-noise level (-68 dB), and, consistent with the discussion of single-surface vibration above, there was no change in the reported vibration amplitude as a function of the distance from the membrane (from -32 to $+32$ μm).

The predictions of Eq. (5) were compared to our experimental data obtained with two surfaces. The values needed for Eq. (5) were the modulation index (determined from the vibration of the front surface when focused on it), the amplitude ratio of the two signals (which varies as the laser is focused at different planes) and their relative phase, ψ_0. The distance between both surfaces was known within a precision of $+/-1$ μm, which was not accurate enough to determine the phase. The phase was a free parameter in the analysis, chosen in order to fit the experimental data.

The ratio c/a was found using the measured carrier levels from the two surfaces together, and the measurement of the optical sectioning curve (carrier level as a function of distance from the focal plane) from a single surface (Fig. 2). The ac signal at the demodulator is given by $x(t)$ of Eq. (4), and the carrier level corresponds to the power in this signal [proportional to $x(t)^2$]. In the case at hand, $\omega_{cC} = \omega_{cA}$. Therefore, the theoretical two-surface carrier power as a function of distance from the focal plane (theoretical two-surface optical sectioning curve) is

$$\text{carrier power (dB)} = \text{constant} + 10\log_{10}(a^2 + c^2 + 2ac\cos(\psi_0)), \quad (6)$$

where a and c were functions of distance, $a = a(z)$, $c = c(z)$. We have assumed that each could be described by the square root of the carrier power vs distance curve with shape as in Fig. 2. ψ_0 was fixed, depending only on the distance between the surfaces. The theoretical two-surface carrier power was calculated using Eq. (6), and compared to the measured two-surface carrier level vs distance curve. The positions of the front and back surfaces were known roughly (± 1 μm) but could be adjusted slightly to improve the fit of Eq. (6) to the measured data. The phase ψ_0 was a fixed but unknown value that was freely adjusted for the best fit. From this fitting procedure $a(z)$, $c(z)$, and ψ_0 were found. Equation (5) was then used to predict the receiver output, $E_o(t)$, where the subscript "o" designates the optical experiments.

Ten experiments with a fixed back surface were performed with different distances between the two surfaces (from 22 to 66 μm). For half of them the back surface was more reflective than the front one (carrier level higher when focused on the back surface than on the front surface). Vibrations were measured for eight frequencies (from 1 to 8 kHz). Theoretical results from Eq. (5), $E(t)$, were compared to the data, $E_o(t)$, and agreed well. Results from several experiments are presented below. The first two correspond to low-modulation-index cases, one with a back surface of higher reflectivity than the front surface and one with the front surface more reflective. We have seen that the effect of competition in the low-modulation-index case is on the fundamental frequency component, without introducing distortion. This held true in the optical experiments, and therefore we emphasize the fundamental component in the analysis of these two experiments.

In the first, the front surface was positioned on $z = 0$ μm and the back surface was at 23 μm behind ($z = -23$ μm). The measured carrier level as a function of the distance is presented in Fig. 10(A) (thick curve). It is the composite curve due to the two surfaces. The back surface had higher reflectivity than the front surface. From this curve and knowing what the curve is like for a single surface (measured data in Fig. 2), the amplitudes a and c were extrapolated. The dashed line is the theoretical carrier level obtained from Eq. (6) with $\psi_0 = 100$ deg. The ratio ρ changed from 0.04 at the front surface ($z = 0$ μm) to 0.9 at $z = +13$ μm and to 1 at $z = -12$ μm. For a ratio of 1, the amplitudes of the two signals are equal.

When driven with the loudspeaker at 7 kHz, the motion of the front surface was measured and the modulation index β_A of the front surface was determined to be 0.043. As $\rho(z) = c(z)/a(z)$, $\beta_C = 0$, and ψ_0 and β_A were known, the theoretical expression [Eq. (5)] could be used in order to predict the demodulator output, and this prediction could be compared with the actual demodulator output. Figure 10(B) assembles experimental (line with circles) and theoretical (crosses) demodulator output. Theory and data were similar.

In the second experiment, the distance between the front surface ($z = 0$ μm) and the back surface was 31 μm. The measured carrier level as a function of distance is presented

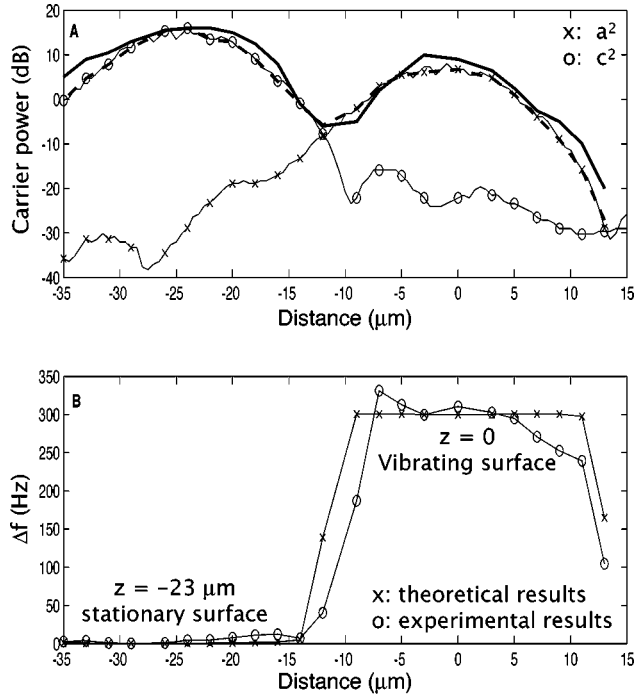

FIG. 10. Interferometer experiment with a vibrating membrane and a stationary back-reflecting surface. The membrane was located at $z=0\ \mu$m and the back surface at $z=-23\ \mu$m. The reflectivity of the back surface was higher. Panel (A): Measured carrier level as a function of distance is shown with a thick line. The carrier level rises and reaches a peak as the plane of the membrane reaches the focal plane. It decreases between the surfaces and reaches a maximum again as the back surface reaches the focal plane. The measured optical sectioning curve (Fig. 2) was used to extrapolate the amplitude of the signals from the two surfaces individually. (The crosses correspond to the extrapolated amplitude of the modulated signal a^2 and the circles to the amplitude of the unmodulated signal c^2). The phase angle ψ_0 between the two carriers could not be measured experimentally and it was selected for best fit. The dashed line is the theoretical carrier level obtained from Eq. (6). Panel (B): Experimentally measured change in the frequency deviation at the modulation frequency as a function of distance from the focal plane (line with circles). Theoretically fitted curve [using Eq. (5)] is shown (line with crosses). ($\beta_A=0.043$, $f_m=7$ kHz, $d=23\ \mu$m, $\psi_0=100$ deg). The theoretical curves fit the measured data quite well.

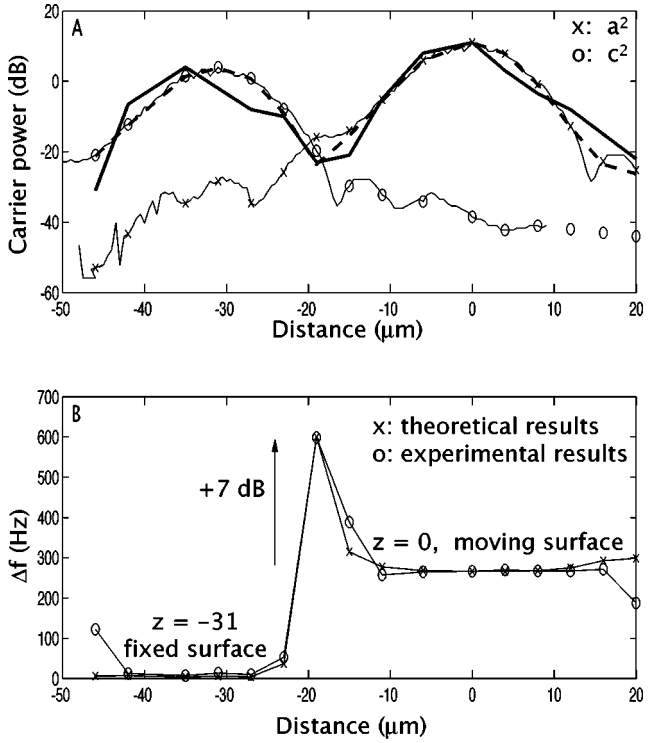

FIG. 11. A second interferometer experiment with a vibrating membrane and a stationary back-reflecting surface. The membrane is located at $z=0\ \mu$m and the stationary back surface is located at $z=-31\ \mu$m. The reflectivity of the front surface was higher. Panel (A): Measured carrier level as a function of distance is shown with a thick line. The dashed line is the theoretical carrier level obtained from Eq. (6). The crosses correspond to the extrapolated amplitude of the modulated signal a^2 and the circles to the amplitude of the unmodulated signal c^2. For this experiment, $\beta_A=0.038$, $f_m=7$ kHz, $d=31\ \mu$m, $\psi_0=166$ deg. Panel (B): Experimental (o) and theoretical (x) frequency deviation (Hz) as a function of distance ($\beta_A=0.038$, $f_m=7$ kHz, $d=31\ \mu$m, $\psi_0=166$ deg). The theoretical results fit the experimental data well, and in particular can account for the peak at $-19\ \mu$m.

in Fig. 11(A). The back surface had lower reflectivity than the front surface. From the extrapolated amplitudes a and c, the theoretical carrier level [Eq. (6)] was determined with $\psi_0=166$ deg (dashed line). The ratio went from 0.004 on the front surface ($z=0\ \mu$m) to 0.1 at $z=+16\ \mu$m and to 0.64 at $z=-19\ \mu$m. When driven with sound, the front surface moved with a small displacement, and produced a low-modulation-index signal ($\beta_A=0.038$, $f_m=7$ kHz). Figure 11(B) compares experimental (line with circles) and theoretical (crosses) data obtained from Eq. (5), knowing ψ_0, the modulation index β_A, $\beta_C=0$, and the values of ρ. An increase of the output of 7 dB (compared to the vibration of the front surface, $z=0$) is observed on $z=-19\ \mu$m. This increase is well explained by the theory. It is due to the relative phase of 166 deg between the signals coming from the two surfaces. Also of note is that even when focused on the back surface, the reported frequency deviation, both theoretical and experimental, although small, was not zero. Therefore, the mobile surface exerts an influence on the measurement at the fixed surface even when the fixed surface has a much larger signal strength. This result is consistent with what was shown in Fig. 5, and reinforces the finding that both relative signal strength and relative β size determine the degree of competition.

With the membrane at the end of a narrow glass tube as a front surface, the modulation index was always low ($\beta_A<0.1$). In order to study a high-modulation-index case, a plastic tube with a bigger diameter membrane was used. We showed above that when the modulation index of the signals is high a competing signal introduces distortion while leaving the fundamental component unaffected. This held true in the optical experiments, and therefore we emphasize the distortion in the analysis of these experiments. When the surfaces were alone, the motion (measured frequency deviation) was almost undistorted (distortion was at least 50 dB down relative to the fundamental), and therefore we attribute the distortion measured when both surfaces were present to the competitive interaction of the two signals. For this experiment, the distance between the two surfaces was $\sim 66\ \mu$m; the modulation index of the front surface, measured at a stimulus frequency of 4 kHz, was 1.77. Figure 12 shows the time-domain signals measured when focused on the mobile front surface [panel (A)] and on the fixed back surface [panel (C)]. The ratio of back/front signal strengths was 0.016 when

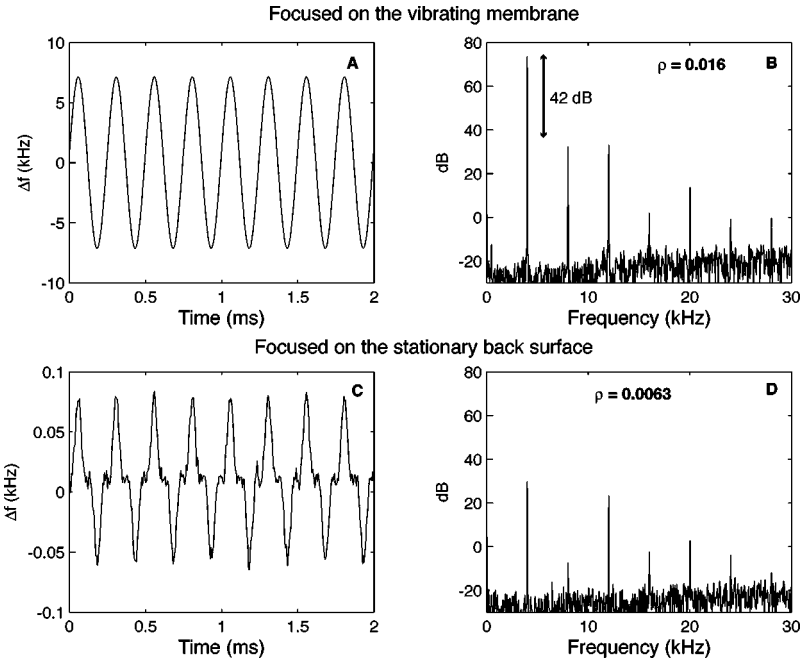

FIG. 12. High-modulation-index case ($f_m=4$ kHz, $\beta_A=1.77$). A larger membrane was used in order to increase its vibration amplitude. The distance between the membrane and the stationary back surface was 66 μm. The upper left curve [panel (A)] is the signal obtained when focused on the front surface, as a function of time; panel (B) is its Fourier transform. The lower curve is the signal obtained with the back surface in focus in the time domain [panel (C)] and in the frequency domain [panel (D)]. The stationary back surface, even though it is far away and its contribution to the total carrier level is small ($\rho=0.016$), can introduce distortion in the demodulator output. Measuring through the vibrating membrane, the stationary surface also appears to vibrate with a distorted waveform.

focused on the front surface, and the ratio of front/back signal strengths was 0.0063 when focused on the back surface. Again, we see that the relatively large motion of the front surface is able to influence the back surface measurement even with a small ratio of signal strengths. The spectra for these two signals are shown in panels (B) and (D). The back surface introduces only a small amount of distortion to the front surface measurement. This is consistent with our expectations, since the back surface is of $\sim$zero β, and the ratio of signal strengths is small.

We conclude the optical experiment section by showing one case in which both front and back surfaces were moving. This was accomplished by threading a glass tube with membrane into the larger plastic tube with membrane and stimulating at 2 kHz. There are no surprises with the results under these conditions, and they serve to round out our experimental results by including a more general case. In Fig. 13, the back surface had $\beta_C=1.14$. The front surface had $\beta_A=1.05$. The ratio of back/front signal strengths was 0.014 when focused on the front surface, and the ratio of front/back signal strengths was 0.032 when focused on the back surface. Panel (A) shows the front surface alone; panel (C) shows the back surface alone (to illustrate the low level of mechanical distortion). Panels (B) and (D) show the distortion introduced by the competing signal of the other surface, when they were separated by 108 μm. [The small change in the fundamental component is difficult to interpret, as the exact position where the motion is measured on the membrane may have changed between panels (C) and (D).] The degree of distortion introduced by the competing signals depends on both the strength of the competing signal and the modulation β of that signal.

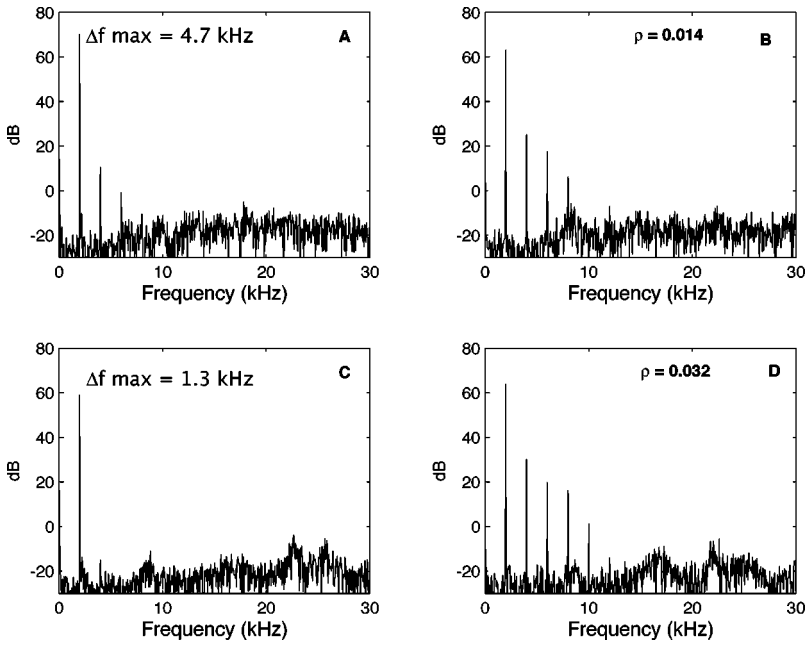

FIG. 13. Two vibrating membranes separated by 108 μm were used in this experiment. Panel (A) shows the Fourier transform of the signal from the front surface alone; panel (C) shows the back surface alone. When measured alone the front membrane vibrated with approximately 11 dB higher amplitude than the back membrane. The second harmonic distortion was low, 60 dB below the fundamental. It was not measurable on the second surface. Panels (B) and (D) show the distortion introduced by the competing signal of the other surface ($\beta_A=1.05$, $\beta_C=1.14$, $f_m=2$ kHz). Panel (B): The front surface is in focus, $\rho=0.014$; panel (D): The back surface is in focus, $\rho=0.032$. When the vibration of each membrane was remeasured with the two membranes in place, the measured amplitude of the first membrane was lowered by about 7 dB (perhaps due to not measuring the same location on the membrane) and its second harmonic distortion increased by 15 dB. The measured amplitude of the second membrane increased by 5 dB and its second harmonic distortion was increased to a level 34 dB below the fundamental. These observations are qualitatively consistent with the theoretical predictions.

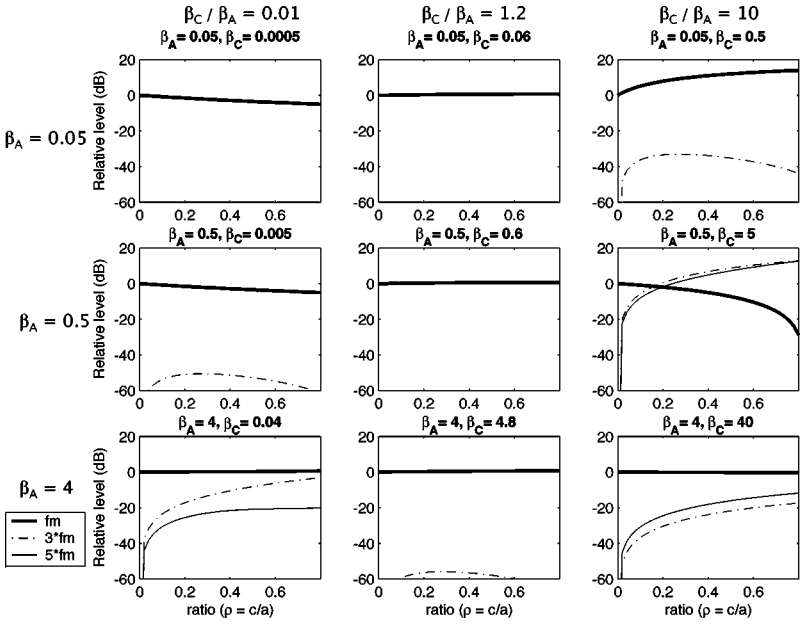

FIG. 14. Effect of a competing signal on the fundamental and harmonic output of the FM demodulator. Change in demodulator output in dB is calculated for various $\rho = c/a$ values and for nine different β combinations. The calculations have been made for $\psi_0 = 0$ deg. The demodulator output at the fundamental frequency can increase, remain unaffected, or decrease sharply depending on the parameters. Only odd harmonics are present when $\psi_0 = 0$ deg. Harmonics are plotted in dB relative to the fundamental level in the absence of competition.

III. BACK TO THE THEORY

From the above, Eq. (5) is very useful to predict the output signal of the FM demodulator when two signals contribute to its input. We conclude the Results section by using Eq. (5) to generate some useful experimental guidelines regarding signal competition. Above, realistic ρ and β values were gleaned from the literature. β values extended from very low modulation index (for low to moderate stimulus levels) to modulation indices at high stimulus levels up to ~ 10. Chinchilla had larger β values than the other species looked at, and guinea pig measurements were always within a low-modulation case, although getting close to the boundary at the highest stimulus levels. Many surfaces in the cochlea are of low reflectivity, the Hensen's cells of guinea pig being a notable exception. If the reflectivities of different surfaces are close to being equal, then the ratio, ρ, is determined largely by the optical sectioning curve and the distance between surfaces. Most surfaces in the cochlea are separated by at least 100 μm, so from Table I (which reports carrier power, so the square root is the relevant quantity) we can see expected ρ values depend on the interferometer and will span values as high as 0.3, and as low as 0.01, with the lower value possible with the low-coherence diode laser of Dalhoff *et al.* and the divided aperture system of Koester *et al.* When the competing surface is of relatively high reflectivity (bone, for example) or is closer, ρ will be accordingly higher. Future measurements that attempt to separate the motion of, for example, tectorial membrane and reticular lamina, will encounter more serious signal competition. The other important parameter is the modulation index ratio. Khanna *et al.* (2000) measured vibrations of Hensen's cell and basilar membrane in an *in vivo* preparation: The basilar-membrane velocity was 10 times smaller, $\beta_{\text{Hensen}}/\beta_{\text{BM}} = 10$

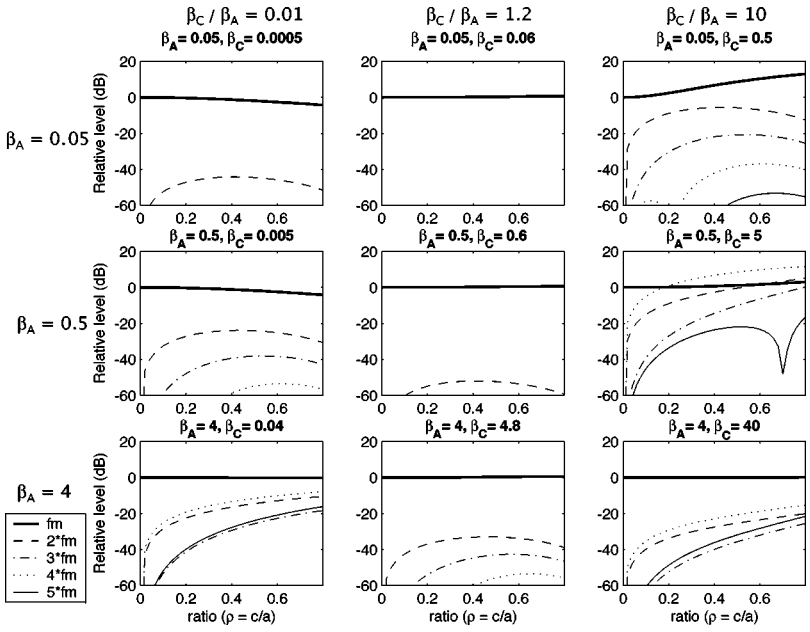

FIG. 15. As in Fig. 14 except calculations have been made for $\psi_0 = 90$ deg. The fundamental component is not affected appreciably except when the modulation index of the competing signal is much higher than that of the primary signal ($\beta_C/\beta_A = 10$). Distortion contains both even and odd harmonics.

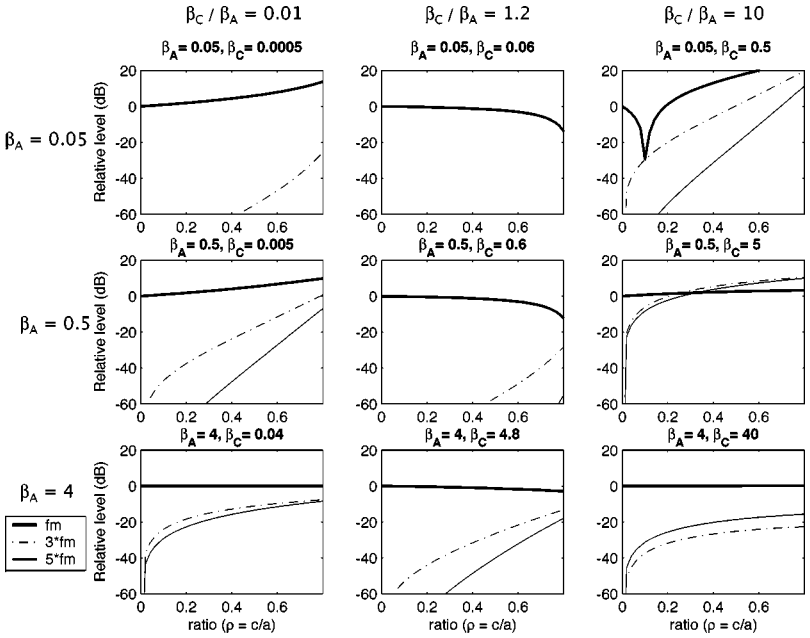

FIG. 16. As in Fig. 14 except calculations have been made for $\psi_0 = 180$ deg. The competing signal introduces the biggest changes for this phase.

(their Fig. 1). In order to address a full range of experimental conditions, we present guidelines that cover a large range of ρ values and three different β_C/β_A ratios.

In Figs. 14, 15, and 16 we show the effect of a competing signal as a function of ρ, and for three different β_C/β_A ratios (left: $\beta_C/\beta_A = 0.01$; middle, $\beta_C/\beta_A = 1.2$; and right $\beta_C/\beta_A = 10$). This generates three plots. These three plots are shown for three values of β_A (top: $\beta_A = 0.05$; middle: $\beta_A = 0.5$; and bottom $\beta_A = 4$). What is plotted is the change in output, $E(t)$, due to the competing signal, reported in dB. The harmonics were zero without competition, and what is plotted is their level relative to the fundamental (without competition). We have seen the strong effect of phase, ψ_0, on the results. Recall that the phase is not under experimental control; it depends on the distance between surfaces. Therefore, we present results for three phase values, 0 deg (Fig. 14), 90 deg (Fig. 15), and 180 deg (Fig. 16). Note that the even harmonics are absent when the phase is 0 deg or 180 deg. This is due to the symmetry of this condition. The 90 deg case shows the more general result, in which both even and odd harmonics are present.

The results from Figs. 14–16 have been distilled in Figs. 17–19, by presenting results in terms of nominally acceptable levels of error in the fundamental and distortion. The acceptable levels chosen were ± 3 dB for the fundamental response, and harmonic levels at least 30 dB down relative to the unchallenged fundamental. These ''threshold'' curves are shown for the same three values of β_A as in Figs. 14–16. On the left axis is $\rho_{\lim}$, the ρ value for which acceptable levels are obtained. (To have a smaller error, ρ has to be less than $\rho_{\lim}$.) If we examine Figs. 17–19 for a ratio of 0.1, we see that for low modulation index ($\beta_A = 0.05$) the errors are ac-

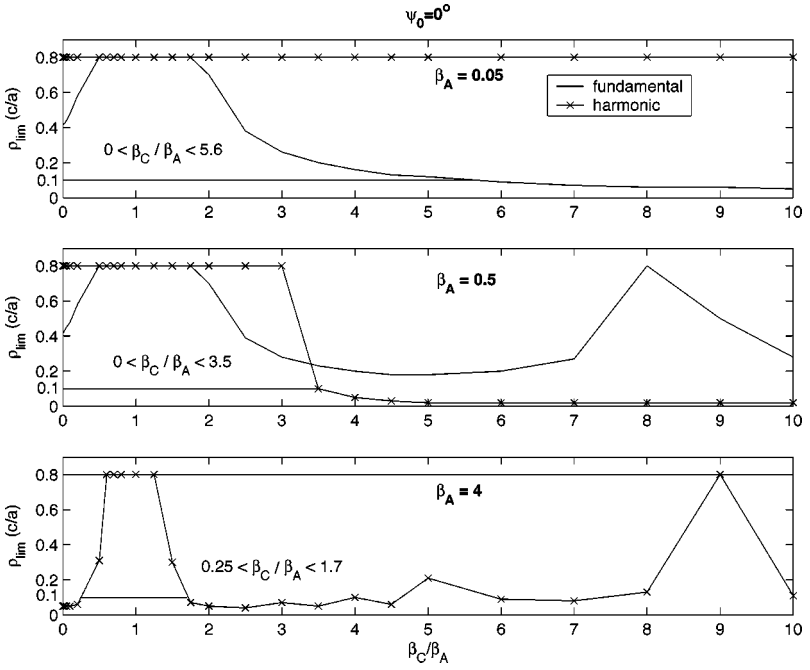

FIG. 17. Ratio ($\rho_{\lim}$) for which the change in the fundamental is $+/-3$ dB and the level of the harmonic components is -30 dB *re*: fundamental. $\rho_{\lim}$ is shown as a function of β_C/β_A for three values of β_A (upper panel, $\beta_A = 0.05$; middle panel $\beta_A = 0.5$; and lower panel, $\beta_A = 4$). The phase is equal to $\psi_0 = 0$ deg. To have an error less than $+/-3$ dB for the fundamental or to have the harmonic component more than 30 dB down compared to the fundamental, ρ needs to be less than $\rho_{\lim}$.

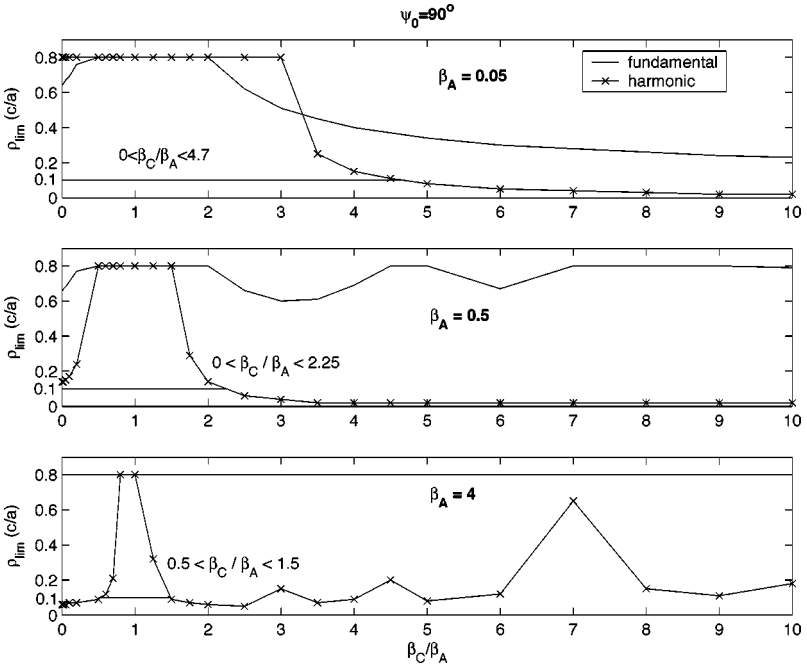

FIG. 18. As in Fig. 17 except $\psi_0 = 90$ deg.

ceptable as long as $\beta_C < 3.5\beta_A$, and for high modulation index ($\beta_A = 4$) the errors are acceptable if β_C is between $0.5\beta_A$ and $1.5\beta_A$, and again are acceptable for large values of β_C ($\beta_C > 7.5\beta_A$). Comparing Figs. 17–19, it is clear that errors in the fundamental component are much greater in the case of $\psi_0 = 180$ deg. Note that if two surfaces vibrate with an arbitrary ρ, with approximately the same amplitude ($\beta_C/\beta_A \sim 1$), and the distance between surfaces is such that $\psi_0 = 0$ deg, no errors or distortion are observed (Fig. 17). In most cases the phase will not be exactly 0 deg, and the phase, being related to distances between cochlear structures, is not under experimental control. However, the physiological basis of measured harmonics could be confirmed by their reproducibility. Comparing Figs. 14–16, the harmonic structure is very sensitive to the ψ_0 value. The ψ_0 value will vary from measurement to measurement, due to slightly different sites and distances. The distortion pattern, as well as the value of the fundamental, will change between the measurements if they are produced by competing signals from out-of-focus planes.

IV. CONCLUSIONS

One factor that governs the optical sectioning capability of an optical system is the objective lens's numerical aperture. Its effect can be described analytically and compared to the split-aperture objective developed by Koester *et al.* The optical sectioning is greatly improved by the split-aperture system.

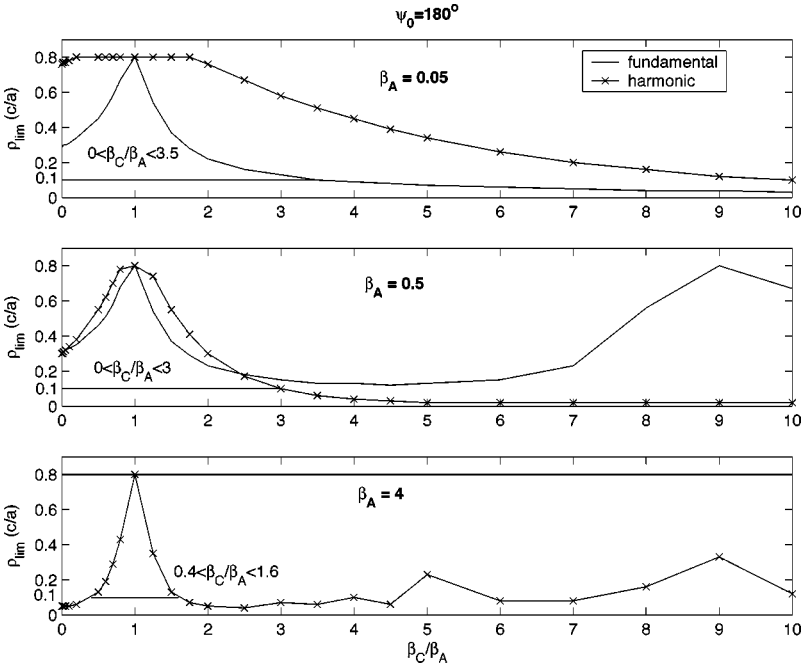

FIG. 19. As in Fig. 17 except $\psi_0 = 180$ deg.

We investigated the effect of a competing signal on the measured vibration. The investigation used both a purely theoretical treatment of FM demodulation [resulting in Eq. (5)] and a simulation of an FM receiver, as well as tests with our FM receiver using competing FM signals that were electronically generated, and finally tests with our entire interferometer/receiver system using optical signals that mimicked a true intracochlear measurement. The most basic result was that the theoretical expression Eq. (5) proved to be useful in predicting actual effects of competition. Beyond that, we found that the qualitative effect of a competing signal depended on the modulation index. When the modulation index was low (corresponding to displacements <25 nm) the competing signal altered the magnitude of the FM receiver output but did not affect its wave shape. When the modulation index was high (displacements>100 nm) the magnitude of the output at the stimulus frequency was resistant to the competing signal even when the ratio was large. However, distortion was present in the receiver output. For both low and high modulation indices the magnitude of the change depended on the phase difference between the two competing signals.

These findings point out that in cochlear vibration measurements made without beads, in order to be sure that the vibration of the selected structure in focus is measured it is important to reduce reflections from out-of-focus structures. A high numerical aperture objective lens attenuates the strength of the reflections from surfaces close to the focal plane, but this attenuation levels off with distance from the focal plane at a level that is not very restrictive. Other means provide attenuation at greater distances from the focal plane. The specialized confocal optics provided by the split-aperture interferometer developed by Koester *et al.* (1994) is one such system. Interferometers using incoherent light, such as that discussed in Dalhoff *et al.* (2001), also provide steep optical sectioning.

ACKNOWLEDGMENTS

This work was supported by the Emil Capita foundation and the NIDCD. Thanks to the reviewers for helpful comments on the manuscript, especially their suggestion that the modulation index be succinctly expressed as a function of displacement amplitude.

[1]When **A** and **C** move with different phases ($\phi_C \neq 0$), the angle φ in Eq. (5) is $\varphi=(\omega_{cC}-\omega_{cA})t+\psi_0-\beta_C\cos(\omega_m t+\phi_C)+\beta_A\cos(\omega_m t)$.

Baghdady, E.J. (**1956**). "Interference rejection in FM receivers," M.I.T. Res. Lab. Electronics, Cambridge, MA, Tech. Rept., **252**, September 24.

Baghdady, E.J. (**1961**). *Lectures on Communication System Theory* (McGraw-Hill, New York), Chap. 19.

Cooper, N.P. (**1999a**). "An improved heterodyne laser interferometer for use in studies of cochlear mechanics," J. Neurosci. Methods **88**, 93–102.

Cooper, N.P. (**1999b**). "Vibration of beads placed on the basilar membrane in the basal turn of the cochlea," J. Acoust. Soc. Am. **106**, L59–L64.

Dalhoff, E., Gärtner, R., Zenner, H.P., Tiziani, H.J., and Gummer, A.W. (**2001**). "Remarks about the depth resolution of heterodyne interferometers in cochlear investigations," J. Acoust. Soc. Am. **110**, 1725–1728.

Khanna, S.M., and Hao, L.F. (**2000**). "Amplification in the apical turn of the cochlea with negative feedback," Hear. Res. **149**, 55–76.

Khanna, S.M., Ulfendahl, M., and Steele, C.R. (**1998**). "Vibration of reflective beads placed on the basilar membrane," Hear. Res. **116**, 71–85.

Khanna, S.M., Koester, C.J., Willemin, J.-F., Dändliker, R., and Rosskothen, H. (**1996**). "A noninvasive optical system for the study of the function of inner ear in living animals," SPIE **2732**, 64–81.

Koester, C.J., Khanna, S.M., Rosskothen, H.D., Tackaberry, R.B., and Ulfendahl, M. (**1994**). "Confocal slit divided-aperture microscope: Applications in ear research," Appl. Opt. **33**, 702–708.

Middleton, D. (**1996**) *An Introduction to Statistical Communication Theory* (IEEE, New York), Chap. 15, pp. 636–642.

Middleton, D., and Spaulding, A.D. (**1981**) "Signals and Interference in FM reception," NTIA Report: 81–87, U.S. Dept. of Commerce.

Nuttall, A.L., Dolan, D.F., and Avinash, G. (**1991**). "Laser Doppler velocimetry of basilar membrane vibration," Hear. Res. **51**, 203–214.

Panter, P.F. (**1965**). *Modulation, Noise and Spectral Analysis: Applied to Information Transmission* (McGraw-Hill, New York).

Ren, T., and Nuttall, A.L. (**2001**). "Recording depth of the heterodyne laser interferometer for cochlear vibration measurement," J. Acoust. Soc. Am. **109**, 826–829.

Robles, L., and Ruggero, M.A. (**2001**). "Mechanics of the mammalian cochlea," Physiol. Rev. **81**, 1305–1350.

Ruggero, M.A., and Rich, N.C. (**1991**). "Application of a commercially manufactured Doppler-shift laser velocimeter to the measurement of basilar membrane vibration," Hear. Res. **51**, 215–230.

Ulfendahl, M. (**1997**). "Mechanical responses of the mammalian cochlea," Prog. Neurobiol. **53**, 331–380.

Willemin, J.F., Dändliker, R., and Khanna, S.M. (**1988**). "Heterodyne interferometer for submicroscopic vibration measurements in the inner ear," J. Acoust. Soc. Am. **83**, 787–795.

Wilson, T. (Editor) (**1990**). *Confocal Microscopy* (Academic, London).